



# Click-crosslinked injectable hyaluronic acid hydrogel is safe and biocompatible in the intrathecal space for ultimate use in regenerative strategies of the injured spinal cord



T. Führmann<sup>a,b</sup>, J. Obermeyer<sup>a,b</sup>, C.H. Tator<sup>c</sup>, M.S. Shoichet<sup>a,b,\*</sup>

<sup>a</sup> Department of Chemical Engineering and Applied Chemistry, University of Toronto, 200 College Street, Toronto, Ont. M5S 3E5, Canada

<sup>b</sup> Institute of Biomaterials and Biomedical Engineering, 160 College Street, Room 530, Toronto, Ont. M5S 3E1, Canada

<sup>c</sup> Krembil Neuroscience Centre, Toronto Western Research Institute, and Department of Surgery, University of Toronto, 399 Bathurst Street, Toronto, Ont. M5T 2S8, Canada

## ARTICLE INFO

### Article history:

Received 14 November 2014

Accepted 26 March 2015

Available online 3 April 2015

### Keywords:

Hydrogel

Spinal cord injury

Drug delivery

## ABSTRACT

Traumatic spinal cord injury (SCI) causes damage and degeneration at and around the lesion site resulting in a loss of function. SCI presents a complex regenerative problem due to the multiple aspects of growth inhibition and the heterogeneity in size, shape and extent of injury. Currently, there is no widely accepted treatment strategy available and delivering biomolecules to the central nervous system remains a challenge. With a view towards achieving local release, we designed a hydrogel that can be injected into the intrathecal space. Here we describe the synthesis and characterization of a click-crosslinked hyaluronic acid hydrogel and demonstrate controlled *in vitro* release of bioactive brain derived neurotrophic factor. Importantly, we demonstrate that this new hydrogel is both biocompatible in the intrathecal space based on immunohistochemistry of the host tissue response and safe based on behavioral analysis of locomotor function.

© 2015 Elsevier Inc. All rights reserved.

## 1. Introduction

Traumatic spinal cord injury (SCI) causes damage and degeneration to glia, neurons, and axons at the lesion site, often resulting in permanent loss of function below the site of injury [1]. However, SCI rarely results in complete tissue disruption at the lesion site, and in many cases there is some functional preservation in segments below the injury, indicating survival of functional axons across the lesion [2]. Therefore, minimally invasive treatment strategies, which enhance preservation of nervous tissue at the injury site and promote regeneration of lesioned tissue, are attractive for SCI.

While drug delivery-based treatment strategies hold great promise, prolonged systemic delivery often leads to unwanted side effects, and some of the more promising therapeutic proteins degrade quickly when delivered systemically, often not reaching the spinal cord in efficacious concentrations [3]. Moreover, many therapeutic molecules are unable to cross the blood–spinal cord barrier (BSCB), which limits their accumulation in the spinal cord

after BSCB repair [4,5]. Strategies that deliver therapeutic molecules locally avoid some of these obstacles. Two techniques have been used to deliver drugs intrathecally to patients: bolus injection, which is simple, results in the drug being dispersed throughout the central nervous system (CNS) by cerebrospinal fluid (CSF) flow [6,7]; and minipump delivery, where the indwelling catheter may either damage the cord or become obstructed or infected [8]. An alternative strategy, which has significant appeal, is local hydrogel injection, where bioactive molecules are dispersed in the hydrogel, thereby localizing the therapeutic molecule to the spinal cord tissue at the site of injection [9,10]. For the latter, injectable hydrogels should be: (1) injectable through a fine gauge needle for minimally invasive insertion; (2) a gel at the injection site to ensure local delivery; (3) degradable/resorbable to avoid a second procedure for biomaterial removal; and (4) bio-inert, eliciting no or minimal toxic or immune response.

Here we describe a hydrogel for intrathecal injection at the site of injury of the spinal cord (see Fig. 1). A small number of injectable hydrogels, categorized as either physical or chemical gels [2], have been used for spinal cord repair, but only a few have been injected intrathecally [9–11]. Some of these hydrogels have proven to be safe and capable of local delivery of therapeutics to the injured spinal cord [9,11]. These physically-crosslinked gels, while obviating the use of potentially cytotoxic crosslinking agents, are often

\* Corresponding author at: Department of Chemical Engineering and Applied Chemistry, University of Toronto, 200 College Street, Toronto, Ont. M5S 3E5, Canada.

E-mail address: [molly.shoichet@utoronto.ca](mailto:molly.shoichet@utoronto.ca) (M.S. Shoichet).

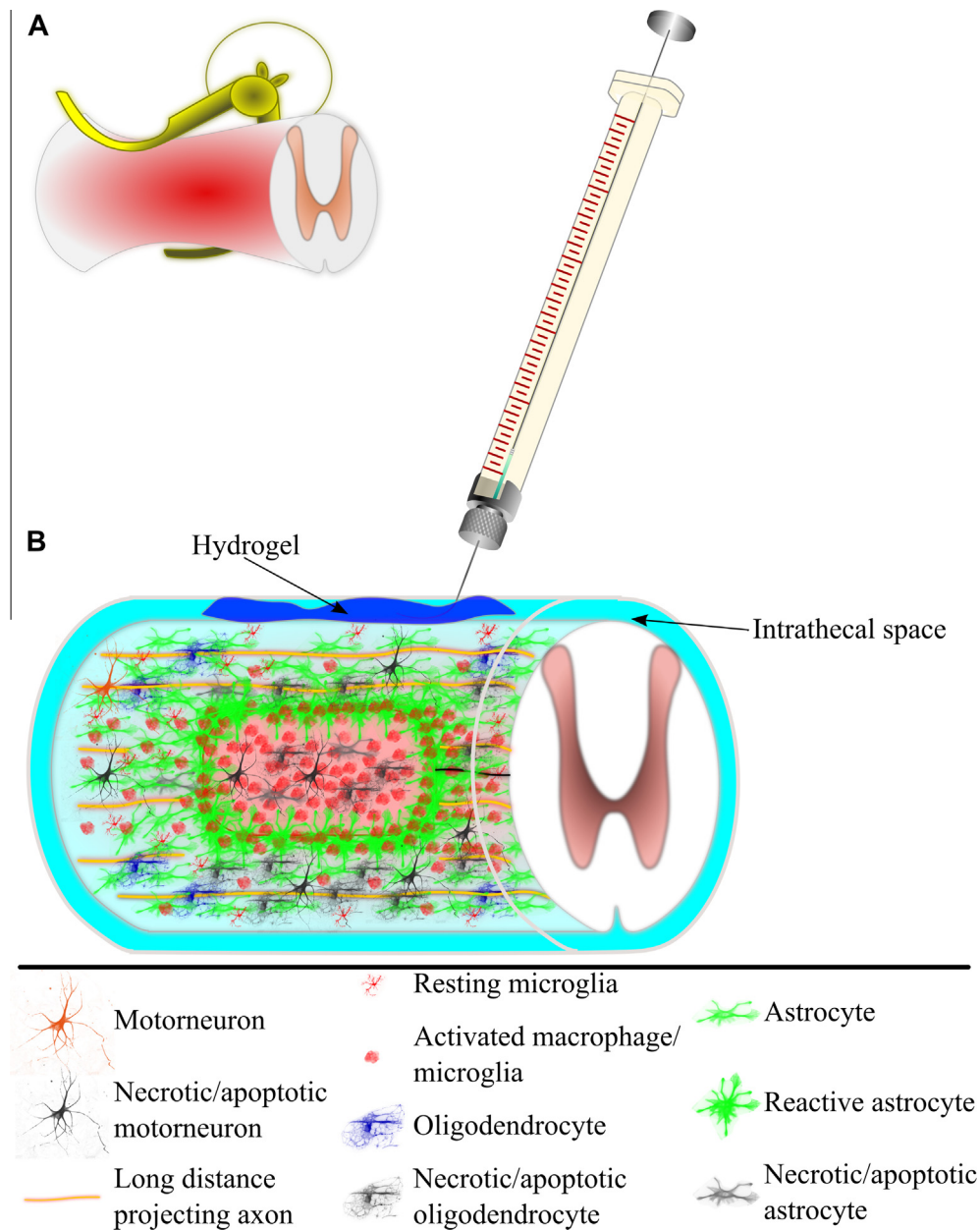


**Fig. 1.** (A) Schematic of the clip compression injury and (B) the hydrogel injection into the intrathecal space on top of the injury. Injection of the hydrogel into the intrathecal space prevents further damage to the spinal cord (compared to direct injection into the tissue).

stable for days to weeks. Chemically crosslinked hydrogels can be tuned to degrade more slowly, thereby providing a route for prolonged biomolecule delivery to the injured spinal cord [12]. However, chemical gels often require potentially cytotoxic molecules for crosslinking, such as coupling agents, catalysts or photoinitiators, thereby potentially compromising biocompatibility [12,13]. Crosslinking via disulfide bond formation overcomes some of these problems, yet the polymer structure can be negatively impacted and side reactions with native proteins are likely [13,14]. Click-crosslinked hydrogels provide the advantages of more stable gels without the disadvantages of cytotoxic coupling agents and side products [15].

Hyaluronic acid (HA) is a major component of the native extracellular matrix [16], but does not form a gel on its own. By reacting HA-furan with poly(ethylene glycol) (PEG) bis-maleimide, a cross-linked hyaluronic acid (xHA) hydrogel is formed based on the Diels–Alder cycloaddition of the HA-furan and PEG-maleimide

[17,18]. Furthermore, HA has been shown to have immunomodulating effects and a hydrogel comprised mainly of HA may be beneficial on its own for tissue regeneration [9,19–21].

We show that this xHA is safe and biocompatible using an experimental animal model of spinal cord injury, and also allows sustained release of bioactive brain-derived neurotrophic factor (BDNF) *in vitro*. To test safety and biocompatibility, the xHA hydrogel was injected intrathecally into both non-injured rats and rats with experimental spinal cord injury using a clinically relevant, moderate clip compression injury model [22,23]. Behavioral and histological analysis demonstrated the safety and biocompatibility of xHA hydrogels, respectively, based on the Basso–Beattie–Bresnahan (BBB) locomotor rating scale [24], and immunostaining of macrophages, microglia, axons and astrocytes. To assess the utility for sustained release of bioactive growth factors, BDNF was encapsulated in poly(lactic-co-glycolic acid) (PLGA) nanoparticles and evaluated for both release, using a BDNF ELISA, and bioactivity

by axonal outgrowth from dorsal root ganglia (DRG). BDNF is compelling for SCI repair as it is neuroprotective, enhances motor neuron axonal outgrowth and stimulates neuronal differentiation from adult neural stem cells [25–29].

## 2. Material & methods

### 2.1. Synthesis and characterization of HA-furan

Furan-modified HA (HA-furan) derivatives were synthesized as described previously [13]. Briefly HA (0.40 g, 1.02 mmol,  $2.34 \times 10^5$  g/mol, Kikkoman Biochemifa, Tokyo, Japan) was dissolved in 40 mL of 2-(N-Morpholino)-ethanesulfonic acid (MES) buffer (100 mM, pH 5.5, Fischer Scientific, Ottawa, Canada) to which 4-(4,6-Dimethoxy-1,3,5-triazin-2-yl)-4-methylmorpholiniumchloride (DMTMM, Sigma–Aldrich, Oakville, Canada) was added in a 2 M ratio (0.56 g, 2.04 mmol, relative to the –COOH groups in HA) and stirred for 10 min. Furfurylamine (Acros Organics, Geel, Belgium) was added dropwise in a 1 M ratio (94.4  $\mu$ l, 1.02 mmol, relative to the –COOH groups in HA). The reaction was conducted at room temperature for 24 h, dialyzed against 0.1 M sodium chloride in distilled water for 3 days (MW cut-off 12–14 kDa), sterile-filtered through a 0.22  $\mu$ m PES filter (Nalgene, Rochester, NY, USA), and lyophilized under sterile conditions. The degree of substitution (DS) was determined from  $^1\text{H}$  NMR spectra by comparing the ratio of the areas under the proton peaks at 6.26, 6.46, and 7.65 ppm (furan protons) to the peak at 1.9 ppm (*N*-acetyl glucosamine protons of HA).  $^1\text{H}$  NMR spectra were recorded in  $\text{D}_2\text{O}$  on a Varian Mercury-400 MHz NMR spectrometer (Palo Alto, CA) (see Supplemental Fig. 1).

### 2.2. Synthesis of xHA hydrogels

xHA hydrogels were synthesized by reacting 10 mg of HA-furan (DS 55%, 13.2  $\mu$ mol of furan) with 7, 10, 13.7 and 20 mg of bis-maleimide-poly(ethylene glycol) ((MI)<sub>2</sub>PEG, 3 kDa, 4.6  $\mu$ mol of maleimide, RAPP Polymere GmbH Tübingen, Germany) crosslinker in 960  $\mu$ l of Dulbecco's phosphate buffered saline (DPBS, Sigma–Aldrich). We determined 7 mg of (MI)<sub>2</sub>PEG to be suitable for further investigations by testing how well the hydrogel is injectable using a 30G needle (see Table 1). The final concentration of HA-furan and (MI)<sub>2</sub>PEG (furan/MI 1:0.5) in the hydrogels for rheology, swelling, BDNF release and *in vivo* investigations was 0.96% and 0.73% w/v, respectively. Samples were allowed to gel at 37 °C for a designated time.

### 2.3. Rheology

The viscoelastic mechanical properties of the xHA hydrogels (10 mg of HA-furan with 7 mg of (MI)<sub>2</sub>PEG) were measured with an AR-1000 rheometer fitted with a 60 mm, 1° acrylic cone using parallel plate geometry (TA Instruments, New Castle, DE) at a gap size of 20  $\mu$ m ( $n = 6$ ). To quantify the gelation time of xHA at 37 °C, oscillation experiments were performed to measure the shear storage modulus ( $G'$ ) and the loss storage modulus ( $G''$ ) as a function of time (over 6 h) at a frequency of 1 Hz. The gelation point is the time at which  $G'$  equals  $G''$ . A frequency sweep was conducted from 0.1 to 10 Hz at 1% strain to determine  $G'$  followed

**Table 1**  
Injectability of xHA hydrogels (10 mg HA-furan) at different time points (++: easily injectable; +: injectable; -: not injectable).

Time/mass of MI <sub>2</sub> -PEG	20 mg	13.7 mg	10 mg	7 mg
4 h	++	++	++	++
8 h	+	+	++	++
16 h (overnight, ON)	–	–	+	+

by a stress sweep test to confirm that the frequency and strain were within the linear viscoelastic region. Sample evaporation was minimized using a solvent trap.

### 2.4. Swelling properties of xHA

To examine swelling properties, xHA hydrogel samples (100  $\mu$ l) were synthesized in pre-weighed vials as described above and accurately weighed ( $M_0$ ). Samples ( $n = 3$ , with 8 gels investigated each time) were then incubated in 500  $\mu$ l of DPBS at 37 °C. DPBS was removed at 8, 24 and 96 h and the mass ( $M_t$ ) measured. The buffer was replenished and the swelling ratios ( $M_t/M_0$ ) determined.

### 2.5. *In vivo* biocompatibility study

All animal procedures were performed in accordance with the Guide to the Care and Use of Experimental Animals (Canadian Council on Animal Care) and protocols were approved by the Animal Care Committee of the Research Institute of the University Health Network. 39 female Sprague Dawley rats (260–350 g; Charles River, Montreal, QC) were used to assess the effects of pre-gelled (overnight at 37 °C) xHA injected into the intrathecal space in terms of behavioral function and immunohistochemical responses ( $n = 4$ /group and time point). Three groups were compared: (I) non-injured animals receiving 10  $\mu$ l of xHA; (II) injured animals receiving 10  $\mu$ l of xHA; and (III) injured animals receiving 10  $\mu$ l of aCSF. Untreated animals were used as qualitative controls for histology only ( $n = 3$ , Supplemental Fig. 2). The intrathecal injections were performed as described previously [10]. Briefly, animals were anesthetized and subjected to a laminectomy at level T2. The spinal cord was either left intact (group I) or moderately injured by cord compression with a 21 g modified aneurysm clip for 1 min (groups II and III), as described previously [23]. The dura was punctured with a 30G needle caudal to T2, and 10  $\mu$ l of sterile xHA or aCSF were injected into the intrathecal space using a customized 30G, 22 mm long blunt needle attached to a 10  $\mu$ l Hamilton syringe. See Fig. 1 for a schematic of the clip compression and the hydrogel injection. After closing the overlying muscles, fascia and skin, rats were placed under a heating lamp and allowed to recover. Animals were sacrificed at 1, 14 and 28 days after surgery and transcardially perfused with 4% PFA in 0.1 M phosphate buffer (PB, pH 7.4). Spinal cords were harvested and cryoprotected with 20% sucrose in 0.1 M PBS. Segments of spinal cord (1.5 cm long), centred around the lesion site, were snap-frozen using isopentane over dry ice and longitudinal cryosections (20  $\mu$ m thick) were prepared. Sections were serially mounted onto adjacent SuperFrost-Plus slides (such that sections on the same slide were obtained from tissue 300  $\mu$ m apart) and stored at –80 °C.

### 2.6. Immunohistochemistry

After fixation, samples were processed for immunocytochemical staining as described previously [30]. Primary antibodies were diluted in 0.1 M PBS and incubated with the preparations overnight at room temperature. The following polyclonal antibodies were used: anti-glial fibrillary acidic protein (GFAP, 1:2000, DAKO) and anti-Iba1 (1:1000, Wako) as well as the following monoclonal antibodies: anti-ED1 (1:500, Santa Cruz) and anti-neurofilament 200 kDa (1:2000, Sigma–Aldrich). Primary antibodies were detected by a combination of secondary antibodies for 2.5 h at RT: Alexa Fluor 488 goat anti-rabbit IgG (1:500, Life Technologies) and Alexa Fluor 546 goat anti-mouse IgG (1:500, Life Technologies). Nuclei were counterstained with 4',6-Diamidino-2-Phenylindole (DAPI, Life Technologies, Burlington, ON).

## 2.7. Morphological analysis

Overviews of the lesion site were taken on an inverted Olympus laser scanning confocal microscope at 200 $\times$  magnification using a motorised stage. The same settings were used for each antibody across the different groups. Axon regeneration/sparing, inflammatory response and gliosis were estimated by quantifying the number of NF200-positive axons crossing the midline of the lesion or the Iba1-positive, ED1-positive and GFAP-positive pixels (respectively) around the lesion site in at least 6 sections/animal. The rostral and caudal edges of the area of interest were determined by the lesion border and the lateral sides by the width of the spinal cord section. ED1, Iba1 and GFAP immunoreactivity were assessed by counting the number of positive pixels after the images were converted to black and white using the same threshold between groups for each antibody and using ImageJ software. Data was standardized to the area of tissue analyzed and plotted as the number of positive pixels/ $\mu\text{m}^2$ . The % of lesion volume was calculated as the area of the cavitated region divided by the total area of the spinal cord cross section according to the GFAP-staining. See Fig. 2 for a schematic of the image analysis.

## 2.8. Functional behavior analysis

General locomotor performance was evaluated weekly for 4 weeks ( $n = 4/\text{group}$ ) using the Basso, Beattie and Bresnahan (BBB) scoring scale [24]. Each hind limb was ranked by two blinded observers and the average used for statistical analysis.

## 2.9. Preparation of BDNF nanoparticles

BDNF PLGA nanoparticles were prepared by a water/oil/water (W/O/W) double emulsion procedure. To create the oil phase, 120 mg of PLGA 50/50 (Sigma–Aldrich, St. Louis, MO) and 4 mg of  $\text{MgCO}_3$  (Sigma–Aldrich, St. Louis, MO) were dissolved in 0.9 mL of dichloromethane (DCM). The inner aqueous phase consisted of 100  $\mu\text{l}$  of aCSF, 12 mg of bovine serum albumin (BSA) (Sigma–Aldrich, St. Louis, MO), and 10  $\mu\text{g}$  of BDNF (Peprotech, Rocky Hill, NJ). The two solutions were added together, vortexed for 10 s and emulsified under sonication (Vibracell VCX 130, Sonics and Materials) for 2 min using a 3 mm probe at 20% amplitude. To this emulsion, 3 mL of 2.5% polyvinyl alcohol (PVA) solution was added and the mixture was vortexed for 10 s and

sonicated for 2 min at 30% amplitude. The emulsion was immediately added to a 31.5 mL bath of 2.5% PVA solution under magnetic stirring at 125 rpm for 16 h. The hardened nanoparticles were collected and washed by ddH<sub>2</sub>O using centrifugation (41,000 $\times$ g at 15  $^\circ\text{C}$  for 10 min) for 4 cycles. The nanoparticles were snap frozen in liquid nitrogen in a vented conical tube and lyophilized. They were stored at  $-20\text{ }^\circ\text{C}$  until use. Encapsulation efficiency of the nanoparticles was determined by sandwich ELISA assay (Promega, Madison, WI) after dissolving the nanoparticles in 0.05 M NaOH.

## 2.10. Preparation of xHA composite hydrogels

A slurry of BDNF-loaded PLGA nanoparticles in DPBS containing (MI)<sub>2</sub>PEG was added to a HA-furan solution to produce a composite hydrogel of 0.96% HA-furan, 0.73% (MI)<sub>2</sub>PEG and 10 wt% PLGA (xHA/PLGA/BDNF).

## 2.11. In vitro release of BDNF from xHA/PLGA/BDNF

A 100  $\mu\text{l}$  aliquot of the xHA/PLGA/BDNF mixture was injected into the bottom of Eppendorf tubes and incubated at 37  $^\circ\text{C}$  for 10 min to ensure gelation. To each tube, 900  $\mu\text{l}$  of aCSF (0.01% BSA) was added, approximating the ratio of xHA to CSF that is expected *in vivo* by injection into the intrathecal space of a rat. These samples were incubated at 37  $^\circ\text{C}$  on an orbital shaker and aCSF was fully removed and replaced with fresh aCSF at  $t = 1\text{ h}$ , 3 h, 1 d, 3 d, 10 d, 14 d, 21 d, and 28 d. A BDNF ELISA assay (Promega, Madison, WI) was used to determine the concentration of BDNF in the aCSF that was removed at each time point ( $n = 3$ ). Artificial cerebral spinal fluid (aCSF, pH 7.4) mimicked the physiologic ion concentrations of the cerebrospinal fluid and consists of: 148 mM NaCl, 3 mM KCl, 0.8 mM  $\text{MgCl}_2$ , 1.4 mM  $\text{CaCl}_2$ , 1.5 mM  $\text{Na}_2\text{HPO}_4$ , 0.2 mM  $\text{NaH}_2\text{PO}_4$ , and 0.1 mg/ml BSA [10].

## 2.12. BDNF bioactivity by dorsal root ganglia (DRG) bioassay

The bioactivity of BDNF released over 28 days was determined using a DRG assay as described previously [31]. All animal procedures were performed in accordance with the Guide to the Care and Use of Experimental Animals (Canadian Council on Animal Care) and protocols were approved by the Animal Care Committee at the University of Toronto. Rat embryo DRG (E17

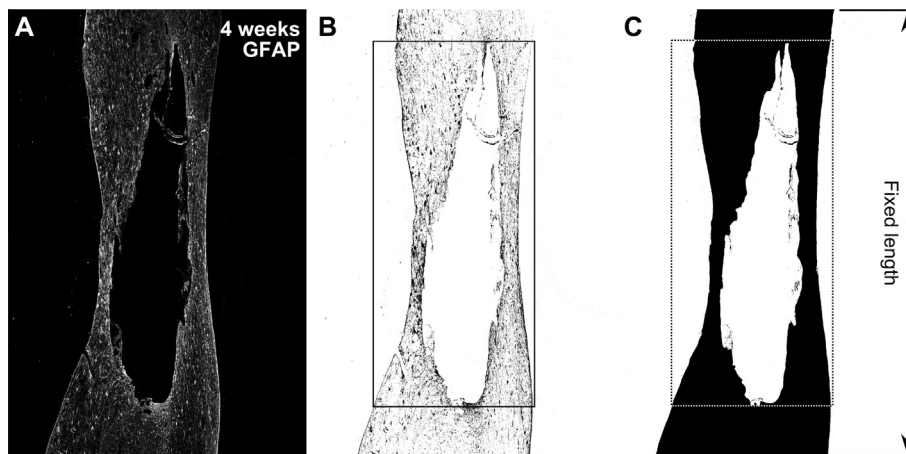


**Fig. 2.** Schematic of the image analysis. (A) The original image was converted into (B) a black and white image using the same threshold for each section and the number of positive (black) pixels in the area of interest (black box) counted. See Figs. 5,6 and 8 for higher magnification images of the threshold used. The amount of positive staining was standardized to the area of tissue analyzed (black area in dotted box, C). The % of lesion volume was calculated as: lesion volume [%] = lesion area/(total tissue area + lesion area)  $\times$  100%. While the length of the section overview was standardized, the width depended on the section itself.

female Sprague–Dawley rats,  $n = 3$ ) were removed and pooled in media comprised of neural basal media supplemented with 2% B-27 serum-free supplement, 1% penicillin–streptomycin, and 1% L-glutamine (Life Technologies). The DRG were then placed on 12 mm diameter glass coverslips coated with poly-D-lysine (50  $\mu\text{g}/\text{mL}$ ) and laminin (5  $\mu\text{g}/\text{mL}$ ) in a 24-well plate. Each release sample replicate was tested on a separate plate. All wells contained 3 DRG and were treated with 0.5 mL of media and 0.5 mL of the BDNF release study supernatant (10, 14, 21, and 28 d). For the controls, 0.5 mL media and 0.5 mL of aCSF (without BDNF) were added to the wells. The DRG were grown for 48 h at 37 °C and 5% CO<sub>2</sub>, fixed with 4% paraformaldehyde (PFA) and processed for immunocytochemistry as described below. The DRG were imaged using an inverted confocal laser scanning microscope (Olympus FV1000). Neurite outgrowth area was calculated by subtracting the cell body area from the total area of the DRG neurite outgrowth. To account for any differences in cell body size the neurite outgrowth area was standardized to the cell body area for statistical analysis. Neurite outgrowth of the released BDNF at different time points was compared to BDNF controls to assess bioactivity.

### 2.13. Statistical analysis

For the DRG outgrowth assay, combined data are plotted as mean + standard deviation (SD). Neurite outgrowth area for each well (containing 3 DRG) was averaged and compared to the control DRG on the same plate using a paired *t*-test.

For *in vivo* studies, data are plotted as mean  $\pm$  standard error of the mean (SEM). For lesion volumes, data were compared by a *t*-test and for multiple comparisons between pairs of means for behavioral and immunohistochemistry analyses, data were compared by an analysis of variance (ANOVA) followed by a Bonferroni's test. *p* values of <0.05 were regarded as significant (\* $p < 0.05$ , \*\* $p < 0.01$ ). All tests were performed using statistical software GraphPad Prism version 5.0.

## 3. Results and discussion

### 3.1. Hydrogel characterization

To be a useful vehicle for intrathecal injection, the hydrogel must be injectable by a minimally-invasive method, low swelling to avoid compression of the spinal cord, cytocompatible, and stable enough to ensure sustained delivery over the desired period of time. We tested injectability, time to gelation and swelling *in vitro* before investigating the biocompatibility *in vivo*.

We tested the injectability of xHA with different amounts of the PEG-crosslinker and different pre-gelation times of 4, 8 and 16 h (overnight). As shown in Table 1, all hydrogels were easily injectable through a 30-gauge syringe after 4 h of pre-gelation; however, xHA hydrogels with higher amounts of crosslinker were difficult to inject after 8 h and effectively non-injectable after 16 h through the 30-gauge syringe. Therefore, further characterizations were performed on the 10 mg HA-furan and 7 mg PEG crosslinker sample. Gelation was tested by rheology with  $G'$  and  $G''$  measured as a function of time [32]. The time to gelation (i.e., where  $G'$  equals  $G''$ ) was approximately 3 h (or  $167.5 \pm 8$  min, mean  $\pm$  SD, Fig. 3A).  $G'$  increased to  $47.8 \pm 3.3$  Pa after overnight gelation at 37 °C. Given the slow gelation of xHA, samples were pre-gelled overnight at 37 °C prior to testing swelling, BDNF release and *in vivo* safety and biocompatibility.

The swelling behavior of xHA hydrogels was characterized by comparing mass before ( $M_0$ ) and after ( $M_t$ ) incubation in DPBS at 37 °C over time. The xHA hydrogel swelled by almost 40% in the first 24 h and by 60% after 96 h, demonstrating a reduced rate of

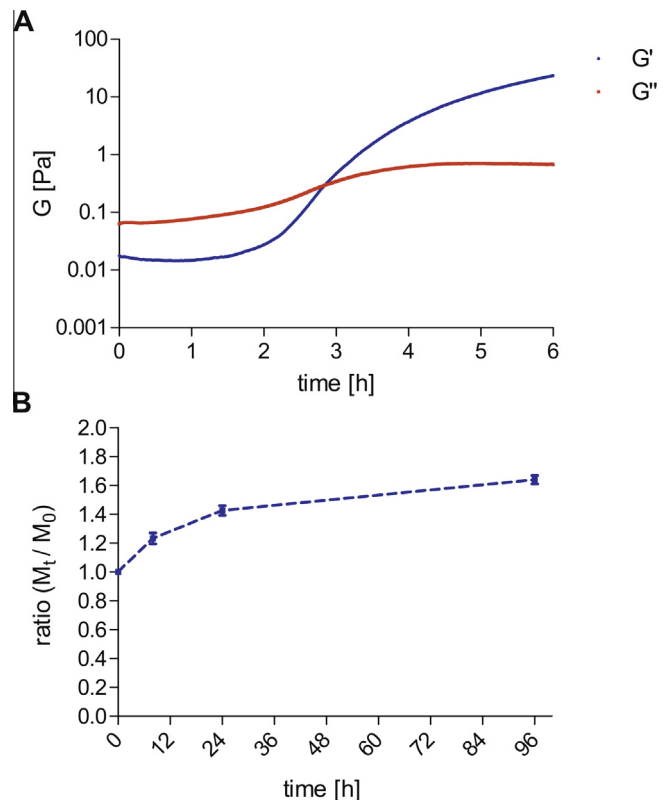


**Fig. 3.** HA-furan can be crosslinked with bis-maleimide-PEG. (A) Rheology demonstrates that the xHA hydrogel crosslinks in less than 3 h, at  $167.5 \pm 8$  min (mean plotted,  $n = 4$ ). (B) The hydrogel swells by  $\sim 40\%$  in the first 24 h and then continues to swell slowly until 96 h ( $M_0$ : mass at time point zero;  $M_t$  mass after 8, 24 or 96 h). The data points at 8, 24 and 96 h are significantly different ( $p < 0.05$ ,  $n = 8$ , mean  $\pm$  SD).

swelling after 24 h (Fig. 3B). Importantly, this level of swelling is tolerated in the intrathecal space, as a volume more than twice of that used can be injected into the normal spinal cord [10,33]. While swelling of the cord after injury and the local confinement of the hydrogel might reduce the amount which can be injected safely, no adverse effects were observed here or with another hydrogel [9].

By controlling the furan to maleimide molar ratio, both the mechanical and degradation properties of the resulting Diels–Alder crosslinked hydrogels can be tuned [13]. Our goal was to use a low modulus hydrogel, which could be injected through a fine (30G) needle. While the crosslinking is more efficient at lower pH, we used DPBS (pH 7.0–7.2) since a lower pH can induce tissue damage [34]. Although early admission and treatment of spinal cord injury patients is critical [35], there are often delays until the patient receives appropriate medical care [36]. Therefore, we aimed to develop a hydrogel that can be prepared before surgery but remains stable and injectable for a long period of time. Interestingly, while xHA is a gel in the syringe, the shear-thinning properties of HA enable injection [9]. Overall, xHA met our design criteria of injectable, stable gel after injection, and low swelling.

### 3.2. *In vivo* biocompatibility

Partially pre-gelled xHA hydrogels were injected into the intrathecal space of uninjured animals to test hydrogel biocompatibility and safety. Specifically, gross anatomy and tissue response were characterized in uninjured animals with or without xHA injection in terms of: axons (NF200), immune cells (ED1 and Iba1) and astrocytes (GFAP), at 1 day and 2 and 4 weeks after

injection. Gross morphological investigations indicated that the uninjured spinal cord was unchanged after the injection of xHA, suggesting minimal swelling of the hydrogel after injection. Furthermore, as shown in Supplemental Fig. 2, no differences in terms of axonal, immune and glial response were observed between the cords of animals that had xHA injected vs. no injection, demonstrating the safety of intrathecal hydrogel injection. Since no differences between uninjured animals receiving xHA or no treatment were observed, only injured animals receiving xHA or aCSF were investigated for behavioral outcomes and tissue response.

### 3.3. Functional behavioral analysis

To investigate the effect of xHA on the gait of the animals, motor function was assessed weekly using BBB scoring – the most commonly used and accepted test for recovery of locomotor function after SCI [24]. Fig. 4 shows BBB scores over a 4 week period for spinal cord injured and non-injured animals injected with either artificial cerebrospinal fluid (aCSF) or xHA. All non-injured animals receiving xHA had BBB scores of 21 (the maximal possible score) throughout the study, indicating that neither the surgical technique nor xHA affected neurological function of the animals. After injury, animals receiving aCSF or xHA showed major neurological deficits with only occasional weight supported stepping and no coordination (average BBB score of 10). Animals in both groups recovered slightly over the observed 4 week period to frequent weight supported stepping and occasional forelimb–hindlimb coordination (average BBB score of 12). There was no significant difference between the xHA and aCSF injected spinal cord injured animals in terms of motor function recovery. These results are comparable to a previous study where the effect a physical blend of HA and methylcellulose (MC) on the non-injured or injured spinal cord were investigated [9]. Similarly, no functional deficits were observed using collagen gels or a composite of HAMC and poly(lactide-co-glycolide) (PLGA) nanoparticles [10,37].

Thus, xHA is safe for intrathecal injection as there was no negative functional impact on the animals with uninjured or injured spinal cords. Importantly, the gels were injectable and minimally-swelling.

### 3.4. Tissue morphology

In order to characterize the biocompatibility of xHA vs. aCSF injection, the spinal cord tissue was further characterized for lesion volume, scarring, axonal density, and cell death following injury. Gross morphological investigations directly after dissection showed no differences between injured animals receiving aCSF or xHA. Immunohistochemistry of longitudinal cryosections of the spinal cords show that at 1 d (data not shown) and 14 d post-injury, immune cells appeared in the intrathecal space of animals that received xHA; however, by day 28, neither the cells nor xHA were evident.

To gain greater insight into the host immune response to hydrogel injection, histological analysis of Iba1 (Fig. 5) and ED1 (Fig. 6) were performed at 14 and 28 days. Iba1 is specifically expressed in macrophages/microglia and is upregulated during their activation [38–40]. Immunostaining against Iba1 of spinal cords with clip compression injury demonstrated an intense staining at the injury site and with time this extended further into the lesion penumbra (Fig. 5A–D). Higher magnification images demonstrate the changed morphology of microglia, with most cells around the injury site resembling the rounded, phagocytic morphology similar to macrophages. Microglia and macrophages are morphologically indistinguishable from each other at this stage within the lesion site (white boxes in Fig. 5C and D indicate the location of the higher magnification image). Quantification of Iba1 immunoreactivity demonstrated no differences between animals receiving aCSF or xHA ( $p > 0.05$ , Fig. 5E). Furthermore, microglial activation around the lesion site was higher at 28 days compared to 14 days for animals receiving either aCSF or xHA ( $*p < 0.05$ , Fig. 5E).

Following acute traumatic injuries, ED1 is expressed rapidly in microglia that are engaged in phagocytosis of tissue debris, similar to the invading monocytes/macrophages [39,41]. Therefore, ED1 identifies activated microglia and activated monocytes/macrophages [39,42]. Injured animals showed many ED1+ cells at and around the lesion site (Fig. 6A–D). At 14 days most ED1+ cells were found within and at the lesion site (Fig. 6A and B), whereas at 28 days many ED1+ cells were within the surrounding tissue (Fig. 6C and D). Higher magnification images demonstrated the typical, rounded morphology of

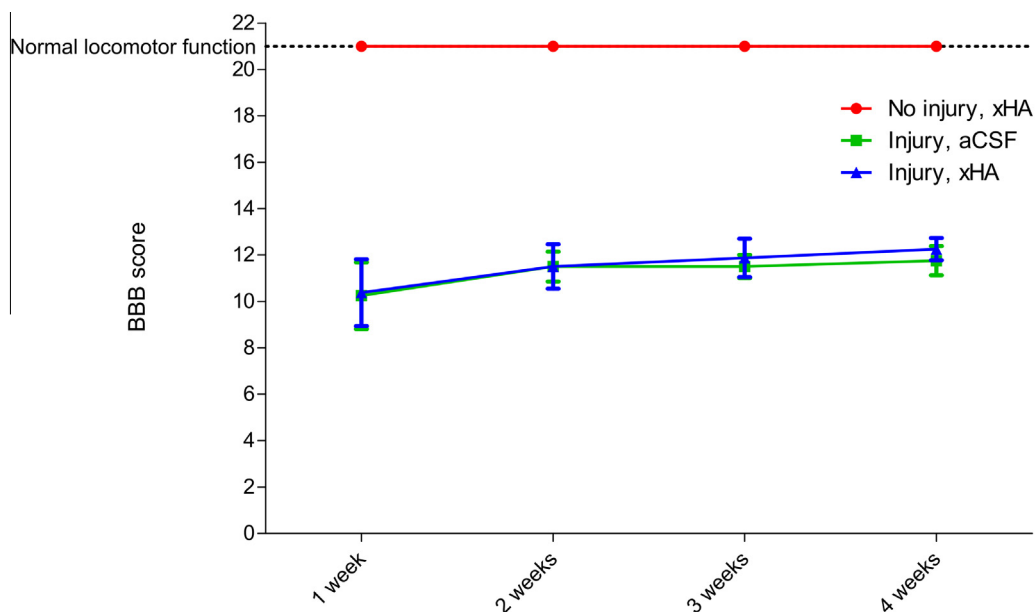


**Fig. 4.** Hydrogel injection does not impair motor function. BBB open field score demonstrates that xHA injection does not lead to impaired motor function in non-injured animals (red line). Furthermore, there was no difference between injured animals receiving aCSF (green line) or xHA (blue line). Data is plotted as mean  $\pm$  SEM ( $n = 4$ ).

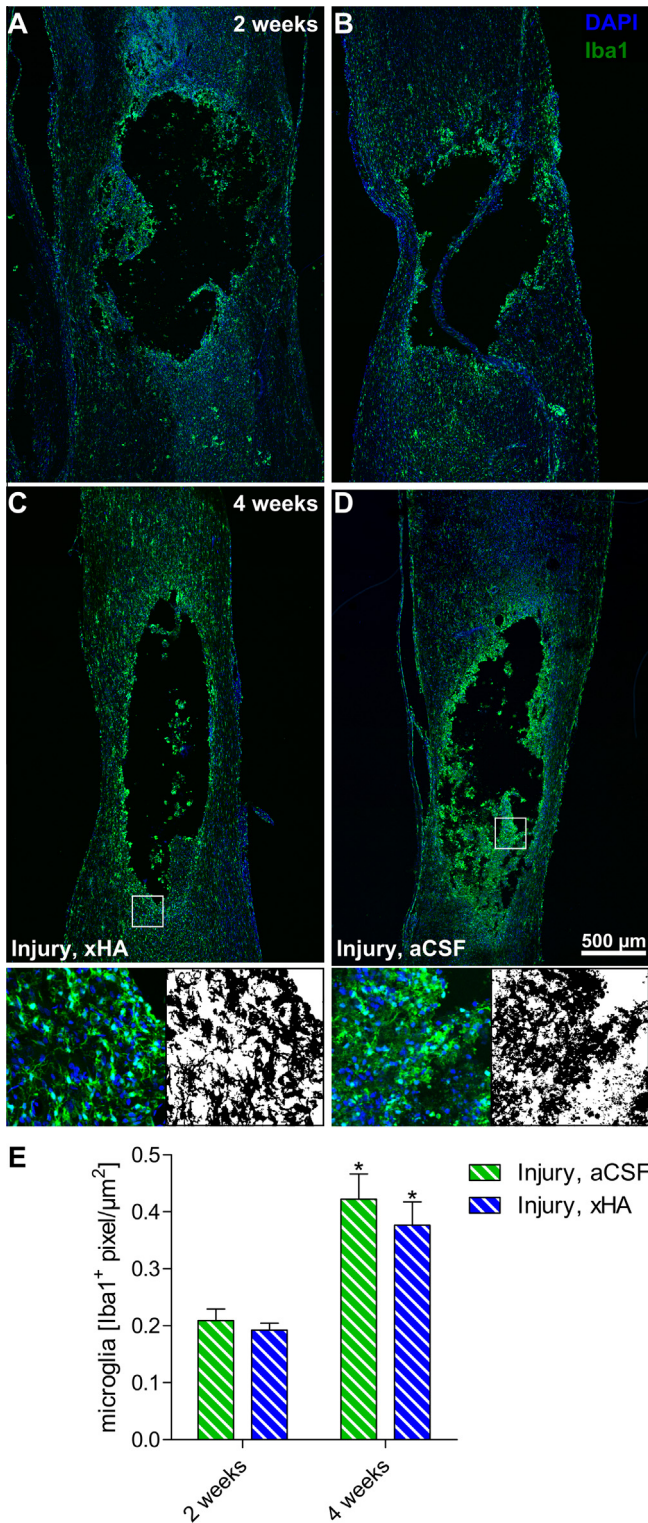


**Fig. 5.** Microglia are activated upon injury and their response increases over time. Iba1 staining (green) demonstrates that microglia are activated upon injury at 2 (A and B) and 4 (C and D) weeks. Higher magnification (white boxes) show that microglia processes hypertrophy or that the whole morphology switches from ramified to rounded. Nuclei were counterstained with DAPI (blue). (E) The pixel counts (black and white images) show that the microglia response increases between 2 and 4 weeks. No differences between injured animals receiving aCSF or xHA were observed. Data is plotted as mean  $\pm$  SEM ( $n = 4$  animals,  $*p < 0.05$  compared to 2 week time point of the same group).

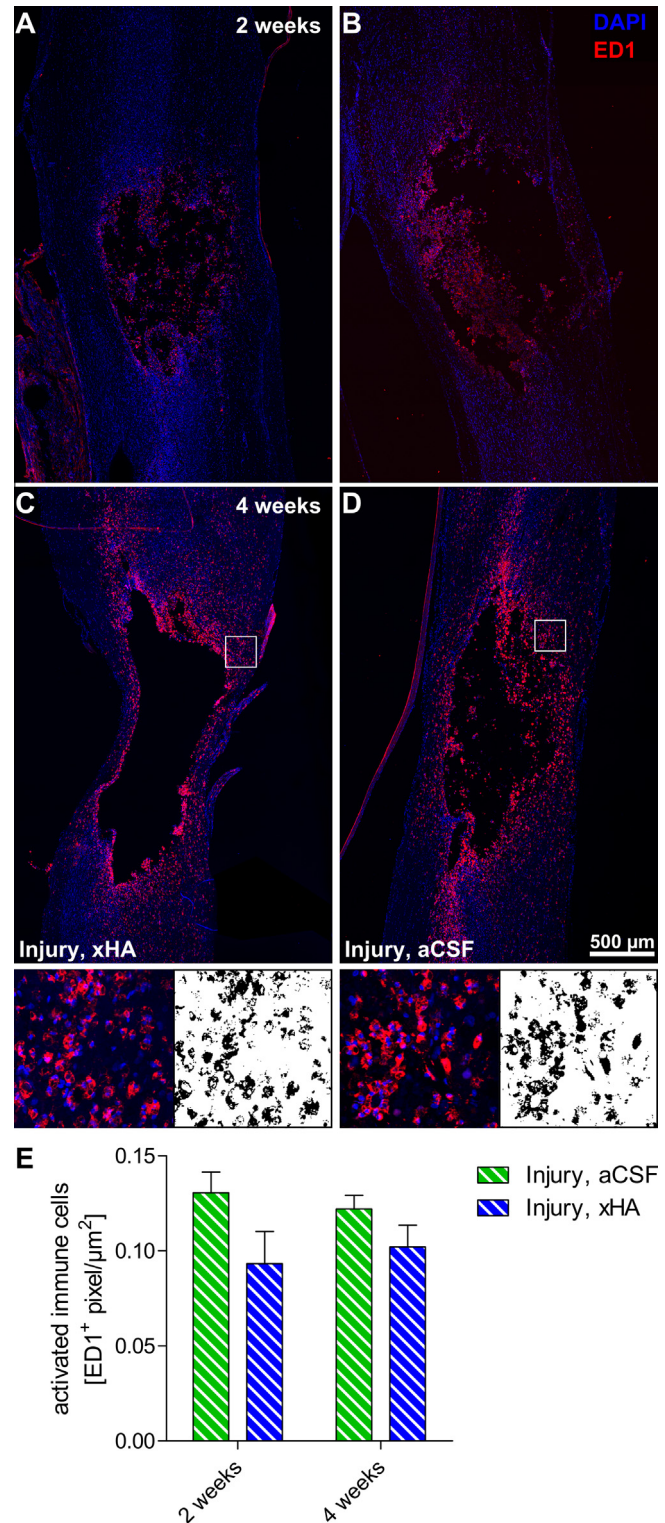


**Fig. 6.** Activated macrophages and microglia accumulate around the lesion site. (A–D) ED1 staining (red) demonstrates the presence of activated macrophages and microglia at and around the lesion site. At 2 weeks (A and B) activated immune cells were predominantly found at the lesion site, whereas at 4 weeks (C and D) they were also found in the lesion penumbra. White boxes indicate location of higher magnification images. Black and white images indicate the threshold used for analysis. Nuclei were counterstained with DAPI (blue). (E) No difference was found between injured animals receiving aCSF or xHA or between groups over time ( $p > 0.05$ ). Data is plotted as mean  $\pm$  SEM ( $n = 4$  animals).

macrophages and phagocytotic microglia (white boxes in Fig. 6C and D indicate the location of the higher magnification image). Quantification of ED1 immunoreactivity demonstrated a trend for a reduced immune response in animals receiving xHA compared with those receiving aCSF; however, this difference was not significant (2 weeks:  $p = 0.08$ , 4 weeks:  $p = 0.19$ ; Fig. 6E).

While there was a trend for a reduced inflammatory response after xHA injection, there was no definite indication of an immunomodulating effect of HA on the lesioned tissue. This contrasts with the previous observation of HAMC where the number of ED1+ immune cell was significantly reduced relative to aCSF [9]. The difference might be due to the higher concentration of HA in the HAMC study (2% previously vs. 0.96% now), the molar mass of HA in HAMC ( $1.6 \times 10^6$  g/mol) vs. that in xHA ( $2.34 \times 10^5$  g/mol) or the presence of PEG in xHA. Fibrin, collagen and HAMC/PLGA composites showed similar results to those of xHA [10,37,43,44]. The similar expression of ED1 at 14 and 28 days is probably due to the shift of ED1+ cells from the lesion core to the surrounding tissue. This matches previous observations, where

amoeboid microglia/macrophage phenotypes were found at the lesion core (primary injury) and later at adjacent areas, which represent regions of ongoing secondary damage [41].

The ED1 immunoreactivity data, together with the increase in Iba1 immunoreactivity, suggest that the immune response persisted for a prolonged time after aCSF or xHA-injection in both injured groups. This is consistent with previous observations in injured animals and is likely associated with the poor prognosis after spinal cord injury [45]. To gain greater insight into the inflammatory response to injected biomaterials, the macrophages may be further distinguished in terms of M1 and M2 [46]; however, this was beyond the scope of this initial investigation.

To more fully understand the impact of xHA injection on axons and astrocytic glial scar formation, immunohistochemistry was performed at 28 days against NF200 (axons, Fig. 7) and GFAP (astrocytes, Fig. 8). Neurofilament positive axons in the white matter carry sensory and motor information between the brain and the

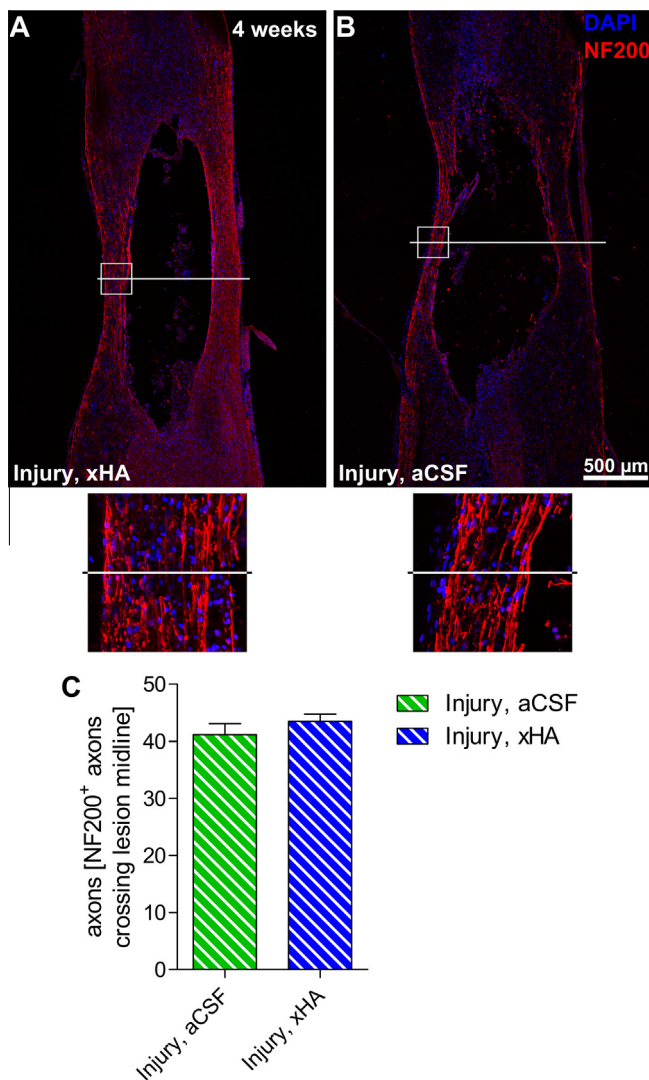


**Fig. 7.** Hydrogel injection did not affect the number of axons traversing the lesion site. (A and B) NF200 staining (red) demonstrates that spared axons laterally transverse the lesion area, whereas no axons regenerated across the lesion core. Nuclei were counterstained with DAPI (blue). Higher magnification images (white boxes) show individual axons. (C) Quantification of axons crossing the midline of the lesion show no difference between animals receiving aCSF or xHA. Data is plotted as mean  $\pm$  SEM ( $n = 4$  animals).

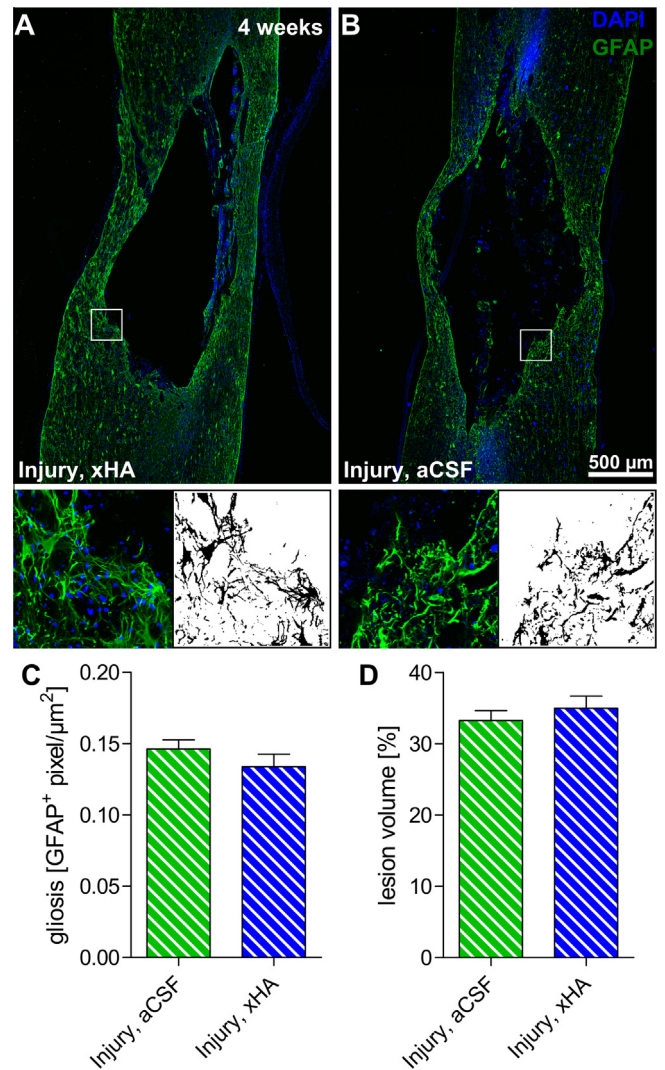


**Fig. 8.** Hydrogel injection did not lead to an increase in lesion volume or astrocyte reactivity. (A and B) GFAP staining (green) shows the border of the scar that forms around the injured tissue. Higher magnification images (white boxes) demonstrate astrocytic morphology at the lesion border. Nuclei were counterstained with DAPI (blue). Black and white images demonstrate the image after the threshold was applied. (C) No differences in GFAP-reactivity were observed for animals receiving aCSF or xHA. (D) Calculated lesion volume according to the GFAP staining shows no differences in cavitation (lesion volume) between injured animals receiving aCSF or xHA. Data is plotted as mean  $\pm$  SEM ( $n = 4$  animals).

periphery, and are often severely damaged by injury [47]. Accordingly, injured animals showed major loss of axons at the lesion site (Fig. 7A and B). Higher magnification images show individual processes of axons (white boxes in Fig. 7A and B indicate location of higher magnification images). Quantification of axonal processes crossing the epicenter of the lesion site show no difference between injured animals receiving aCSF or xHA (Fig. 7C). This indicates that xHA is biocompatible. While these results show the devastating loss of axons after injury, they also demonstrate the preservation of axons peripherally in the subpial rim, as described earlier [1,2].

A prominent hallmark of reactive gliosis is hypertrophy of the astrocytic cell bodies and processes with increased production of the intermediate filament, glial fibrillary acidic protein (GFAP) [48,49]. In injured animals, the usually highly organised cytoarchitecture is disrupted and astrocytes around the lesion site show a reactive morphology with upregulated GFAP and thick interwoven processes (Fig. 8A and B), as demonstrated by the higher magnification images (white boxes indicate the location of higher magnification images). Quantification of GFAP immunoreactivity demonstrates no differences between injured animals receiving aCSF or xHA (Fig. 8C). Furthermore, there was no difference in lesion volume (as a % of total tissue at the lesion site) between injured animals receiving aCSF or xHA (Fig. 8D). While often the total lesion volume (in mm<sup>2</sup>) is shown (see references [50,51] for

detailed protocols), we plotted the percentage of the lesion volume to total tissue, as this gives a better indication of how much of the tissue was lost in a given volume.

Thus, while injury itself results in significant gliosis, axonal loss and immune response, injection of xHA has no negative impact on any of these parameters relative to aCSF injection. This demonstrates that xHA is biocompatible.

### 3.5. *In vitro* release and bioactivity of BDNF

To achieve sustained release, BDNF was encapsulated into PLGA nanoparticles, with an encapsulation efficiency of 47.2% and a loading of 34.6 ng BDNF/mg nanoparticles. BDNF PLGA nanoparticles were dispersed in the xHA hydrogel and then added to aCSF, from which released BDNF was detected by ELISA and for bioactivity with a DRG neurite outgrowth assay. As shown in Fig. 9A, only small amounts of BDNF were released for the first few days, with only  $0.4 \pm 0.1$  ng released after 5 days. A linear sustained release profile ensued, with a total mass of  $229 \pm 27$  ng BDNF released after 28 days, corresponding to  $76 \pm 9\%$  of total protein loaded. The delayed release was expected, since PLGA has been demonstrated to slow the release from hydrogels previously [31,52,53].

The bioactivity of BDNF released from xHA was measured by a neurite outgrowth assay using embryonic rat DRGs. At days 10, 14, 21, and 28, all nanoparticle formulations promoted significantly

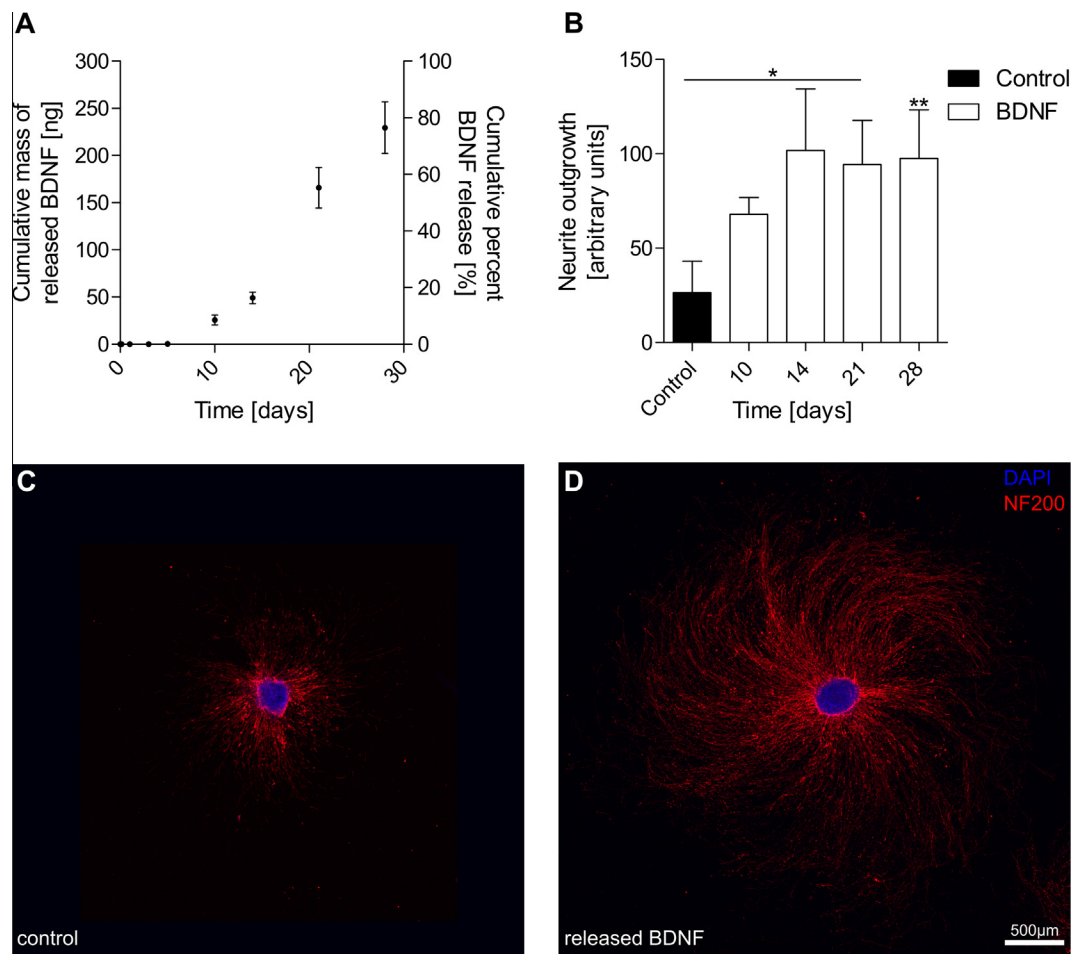


**Fig. 9.** BDNF release from xHA. (A) We observed a delayed BDNF release, with only a few ng released in the first 5 days. Subsequently BDNF showed a sustained release, with 77% of the encapsulated BDNF released at day 28. (B) Histogram of overall neurite outgrowth, standardized to the DRG cell body area. Significantly greater neurite outgrowth was observed with BDNF substituted media. Data is plotted as mean  $\pm$  SD ( $n = 3$ ),  $***p < 0.01$ ,  $*p < 0.5$  compared to control. (C and D) NF200 immunoreactive DRG neurite outgrowth on PLL/laminin-coated coverslips in media without BDNF (control, C) and in media substituted with released BDNF (28 days, D).

greater neurite outgrowth compared to controls ( $p < 0.05$ , Fig. 9B), thereby demonstrating sustained release of bioactive BDNF. The DRG achieved substantial neurite outgrowth over 48 h of culture, generating a relatively symmetrical halo of NF200+ neurites around the cell bodies (Fig. 9C and D).

#### 4. Conclusions

Intrathecal injection of xHA is safe and biocompatible, causing neither functional nor tissue damage. Here we demonstrated methods to synthesize and characterize a chemically crosslinked, minimally swelling, injectable hydrogel comprised of HA-furan and bis-maleimide-PEG for intrathecal delivery to the injured spinal cord. The hydrogel was synthesized based on Diels–Alder cycloaddition without the use of any coupling agent or side reactions. xHA was injected through a fine needle and was visible at the injection site in the intrathecal space for at least 2 weeks. We showed behavioral and histological methods to determine the safety and biocompatibility of xHA after injection into the intrathecal space. Furthermore, we demonstrated sustained release of bioactive BDNF from xHA. In future studies, local, sustained release of bioactive molecules to the injured spinal cord will be investigated in terms of therapeutic benefit.

#### Acknowledgements

We are grateful to Mrs. Rita van Bendegem for tissue processing. We thank Peter Poon for animal surgery, Jennifer Chan for the assistance with immunohistochemistry and fluorescence imaging, Shawn Owen for discussions regarding xHA chemistry and the Fehlings lab for help with animal care. We thank the Canadian Institutes of Health Research (CIHR) for operating funding (to M.S.S.), the CIHR TPRM training grant (to T.F.) and the Natural Sciences and Engineering Research Council (NSERC) graduate student scholarship (to J.O.).

#### Appendix A. Supplementary data

Supplementary data associated with this article can be found, in the online version, at <http://dx.doi.org/10.1016/j.ymeth.2015.03.023>.

#### References

- [1] M.E. Schwab, D. Bartholdi, *Physiol. Rev.* 76 (1996) 319–370.
- [2] D. Macaya, M. Spector, *Biomed. Mater.* 7 (2012), <http://dx.doi.org/10.1088/1748-6041/7/1/012001>.
- [3] R. Pawar, A. Ben-Ari, A.J. Domb, *Expert Opin. Biol. Ther.* 4 (2004) 1203–1212, <http://dx.doi.org/10.1517/14712598.4.8.1203>.
- [4] N.J. Abbott, I.A. Romero, *Mol. Med. Today* 2 (1996) 106–113.
- [5] W.M. Pardridge, *Mol. Biotechnol.* 30 (2005) 57–70, <http://dx.doi.org/10.1385/MB:30:1:057>.
- [6] T.L. Yaksh, K.A. Horais, N. Tozier, M. Rathbun, P. Richter, S. Rossi, et al., *Toxicol. Sci.* 80 (2004) 322–334, <http://dx.doi.org/10.1093/toxsci/kfh168>.
- [7] H. Terada, T. Kazui, M. Takinami, K. Yamashita, N. Washiyama, B.A. Muhammad, *J. Thorac. Cardiovasc. Surg.* 122 (2001) 979–985, <http://dx.doi.org/10.1067/j.mtc.2001.117278>.
- [8] L.L. Jones, M.H. Tuszyński, *Microsc. Res. Tech.* 54 (2001) 317–324, <http://dx.doi.org/10.1002/jemt.1144>.
- [9] D. Gupta, C.H. Tator, M.S. Shoichet, *Biomaterials* 27 (2006) 2370–2379, <http://dx.doi.org/10.1016/j.biomaterials.2005.11.015>.
- [10] M.C. Jimenez Hamann, E.C. Tsai, C.H. Tator, M.S. Shoichet, *Exp. Neurol.* 182 (2003) 300–309.
- [11] M.C. Jimenez Hamann, C.H. Tator, M.S. Shoichet, *Exp. Neurol.* 194 (2005) 106–119, <http://dx.doi.org/10.1016/j.expneurol.2005.01.030>.
- [12] T.R. Hoare, D.S. Kohane, *Polymer* 49 (2008) 1993–2007, <http://dx.doi.org/10.1016/j.polymer.2008.01.027>.
- [13] C.M. Nimmo, S.C. Owen, M.S. Shoichet, *Biomacromolecules* 12 (2011) 824–830, <http://dx.doi.org/10.1021/bm101446k>.
- [14] X.Z. Shu, Y. Liu, Y. Luo, M.C. Roberts, G.D. Prestwich, *Biomacromolecules* 3 (2002) 1304–1311.
- [15] H.C. Kolb, M.G. Finn, K.B. Sharpless, *Angew. Chem. Int. Ed. Engl.* 40 (2001) 2004–2021.
- [16] F.Z. Volpato, T. Führmann, C. Migliaresi, D.W. Huttmacher, P.D. Dalton, *Biomaterials* (2013), <http://dx.doi.org/10.1016/j.biomaterials.2013.03.057>.
- [17] S. Otto, J.B. Engberts, *Org. Biomol. Chem.* 1 (2003) 2809–2820.
- [18] D.C. Rideout, R. Breslow, *J. Am. Chem. Soc.* 102 (1980) 7816–7817, <http://dx.doi.org/10.1021/ja00546a048>.
- [19] W.Y. Chen, G. Abatangelo, *Wound Repair. Regen.* 7 (1999) 79–89.
- [20] K.M. Sheehan, L.B. DeLott, S.M. Day, D.H. DeHeer, *J. Orthop. Res.* 21 (2003) 744–751, [http://dx.doi.org/10.1016/S0736-0266\(03\)00007-X](http://dx.doi.org/10.1016/S0736-0266(03)00007-X).
- [21] A. Roth, J. Mollenhauer, A. Wagner, R. Führmann, A. Straub, R.A. Venbrocks, et al., *Arthritis Res. Ther.* 7 (2005) R677–686, <http://dx.doi.org/10.1186/ar1725>.
- [22] P.C. Poon, D. Gupta, M.S. Shoichet, C.H. Tator, *Spine Phila Pa* 1976 (32) (2007) 2853–2859, <http://dx.doi.org/10.1097/BRS.0b013e31815b7e6b>.
- [23] A.S. Rivlin, C.H. Tator, *Surg. Neurol.* 10 (1978) 38–43.
- [24] D.M. Basso, M.S. Beattie, J.C. Bresnahan, *J. Neurotrauma* 12 (1995) 1–21.
- [25] S. Ahmed, B.A. Reynolds, S. Weiss, *J. Neurosci.* 15 (1995) 5765–5778.
- [26] A.K. Shetty, D.A. Turner, *J. Neurobiol.* 35 (1998) 395–425.
- [27] N. Weishaupt, A. Blesch, K. Fouad, *Exp. Neurol.* 238 (2012) 254–264, <http://dx.doi.org/10.1016/j.expneurol.2012.09.001>.
- [28] B.K. Kwon, J. Liu, C. Lam, W. Plunet, L.W. Oschepok, W. Hauswirth, et al., *Spine* 32 (2007) 1164–1173, <http://dx.doi.org/10.1097/BRS.0b013e318053ec35>.
- [29] H.S. Sharma, in: J.T. Hoff, R.F. Keep, G. Xi, Y. Hua (Eds.), *Brain Edema XIII*, Springer, Vienna, 2006, pp. 329–334. <[http://link.springer.com/chapter/10.1007/3-211-30714-1\\_69](http://link.springer.com/chapter/10.1007/3-211-30714-1_69)> (accessed September 5, 2014).
- [30] I. Buchwalow, V. Samoilova, W. Boecker, M. Tiemann, *Sci. Rep.* 1 (2011) 28, <http://dx.doi.org/10.1038/srep00028>.
- [31] J.C. Stanwick, M.D. Baumann, M.S. Shoichet, *J. Controlled Release* 160 (2012) 666–675, <http://dx.doi.org/10.1016/j.jconrel.2012.03.024>.
- [32] H.H. Winter, F. Chambon, *J. Rheol.* 30 (1986) 367–382, <http://dx.doi.org/10.1122/1.549853>.
- [33] P.V. Turner, T. Brabb, C. Pekow, M.A. Vasbinder, *J. Am. Assoc. Lab. Anim. Sci.* 50 (2011) 600–613.
- [34] J. Guo, H. Su, Y. Zeng, Y.X. Liang, W.M. Wong, R.G. Ellis-Behnke, et al., *Nanomedicine* 3 (2007) 311–321, <http://dx.doi.org/10.1016/j.nano.2007.09.003>.
- [35] M.G. Fehlings, R.G. Perrin, *Injury* 36 (Suppl. 2) (2005) B13–B26, <http://dx.doi.org/10.1016/j.injury.2005.06.011>.
- [36] J. Spinal Cord Med. 31 (2008) 408–479, <http://dx.doi.org/10.1043/1079-0268-31.4.408>.
- [37] M.D. Baumann, C.E. Kang, C.H. Tator, M.S. Shoichet, *Biomaterials* 31 (2010) 7631–7639, <http://dx.doi.org/10.1016/j.biomaterials.2010.07.004>.
- [38] Y. Sasaki, K. Ohsawa, H. Kanazawa, S. Kohsaka, Y. Imai, *Biochem. Biophys. Res. Commun.* 286 (2001) 292–297, <http://dx.doi.org/10.1006/bbrc.2001.5388>.
- [39] W.J. Streit, Q.-S. Xue, *J. Neuroimmune Pharmacol.* 4 (2009) 371–379, <http://dx.doi.org/10.1007/s11481-009-9163-5>.
- [40] D. Ito, K. Tanaka, S. Suzuki, T. Dembo, Y. Fukuuchi, *Stroke J. Cereb. Circ.* 32 (2001) 1208–1215.
- [41] C.A. Mueller, H.J. Schluesener, S. Conrad, T. Pietsch, J.M. Schwab, *J. Neurosurg. Spine* 4 (2006) 233–240, <http://dx.doi.org/10.3171/spi.2006.4.3.233>.
- [42] C.E. Milligan, T.J. Cunningham, P. Levitt, *J. Comp. Neurol.* 314 (1991) 125–135, <http://dx.doi.org/10.1002/cne.903140112>.
- [43] P.J. Johnson, S.R. Parker, S.E. Sakiyama-Elbert, *J. Biomed. Mater. Res. A* 92A (2010) 152–163, <http://dx.doi.org/10.1002/jbm.a.32343>.
- [44] S. Yung, T.M. Chan, *J. Biomed. Biotechnol.* 2011 (2011), <http://dx.doi.org/10.1155/2011/180594>.
- [45] L. Schnell, S. Fearn, H. Klassen, M.E. Schwab, V.H. Perry, *Eur. J. Neurosci.* 11 (1999) 3648–3658.
- [46] R. Shechter, O. Miller, G. Yovel, N. Rosenzweig, A. London, J. Ruckh, et al., *Immunity* 38 (2013) 555–569, <http://dx.doi.org/10.1016/j.immuni.2013.02.012>.
- [47] R.E. Ward, W. Huang, M. Kostusiak, P.N. Pallier, A.T. Michael-Titus, J.V. Priestley, *Neuroscience* 260 (2014) 227–239, <http://dx.doi.org/10.1016/j.neuroscience.2013.12.024>.
- [48] C.P. Barrett, L. Guth, E.J. Donati, J.G. Krikorian, *Exp. Neurol.* 73 (1981) 365–377.
- [49] L.F. Eng, *J. Neuroimmunol.* 8 (1985) 203–214.
- [50] L.B. Jakeman, in: J. Chen, X.-M. Xu, Z.C. Xu, J.H. Zhang (Eds.), *Anim. Models Acute Neurol. Inj.*, Humana Press, 2012, pp. 417–442. <[http://link.springer.com/protocol/10.1007/978-1-61779-782-8\\_37](http://link.springer.com/protocol/10.1007/978-1-61779-782-8_37)> (accessed October 10, 2014).
- [51] *Animal Models of Acute Neurological Injuries II – Injury and Mechanistic Assessments*, Vol. 2, n.d. <<http://www.springer.com/biomed/neuroscience/book/978-1-61779-781-1>> (accessed October 10, 2014).
- [52] M.J. Caicco, M.J. Cooke, Y. Wang, A. Tuladhar, C.M. Morshead, M.S. Shoichet, *J. Controlled Release* 166 (2013) 197–202, <http://dx.doi.org/10.1016/j.jconrel.2013.01.002>.
- [53] Y. Wang, M.J. Cooke, N. Sachewsky, C.M. Morshead, M.S. Shoichet, *J. Controlled Release* 172 (2013) 1–11, <http://dx.doi.org/10.1016/j.jconrel.2013.07.032>.